Scaling Theory of Stretched Polymers in Nanoslits

ARTICLE *in* MACROMOLECULES · OCTOBER 2013

Impact Factor: 5.8 · DOI: 10.1021/Ma4010549

3 AUTHORS, INCLUDING:

Alessandro Taloni
University of Milan
27 PUBLICATIONS **321** CITATIONS
SEE PROFILE

Jia-Wei Yeh
Cornell University
7 PUBLICATIONS **37** CITATIONS
SEE PROFILE

Macromolecules

Article

pubs.acs.org/Macromolecules

Scaling Theory of Stretched Polymers in Nanoslits

Alessandro Taloni,[†,*] Jia-Wei Yeh,[‡] and Chia-Fu Chou*[,‡,§,⊥]

[†]CNR-IENI, Via R. Cozzi 53, 20125 Milano, Italy

[‡]Institute of Physics, Academia Sinica, Nangang, Taipei 11529, Taiwan

[§]Research Center for Applied Sciences, Nangang, Taipei 11529, Taiwan

[⊥]Genomics Research Center, Academia Sinica, Nangang, Taipei 11529, Taiwan

ABSTRACT: We provide a scaling framework describing the different regimes attained by a slit-confined polymer, undergoing an external pulling force $f_{el,slit}$. Linear and nonlinear force−extension relations are discussed in the limit of small and large elongations, resorting to the notion of self-avoiding pancakes. The crossover to a channellike behavior allows to explain the scaling of $f_{el,slit}$ as a function of the confinement h observed in recent tug-of-war experiments. The theoretical analysis provides also a qualitative explanation of DNA relaxation and coil−stretch transition experiments performed in nanoslits.

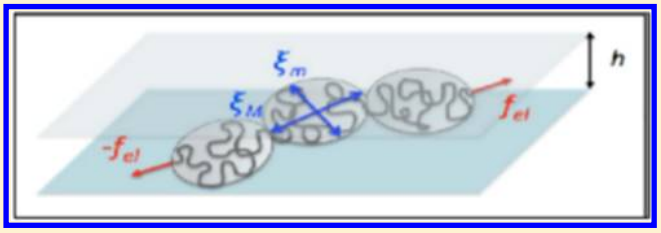

INTRODUCTION

Equilibrium static and dynamical properties of polymers under confinement have been studied for decades.[1−10] The outcomes of such theoretical investigations, often taking the form of scaling relations, only recently have begun to be tested in single molecule experiments. As a matter of fact, the advances in micro- and nanofabrication techniques combined with fluorescence microscopy detection have permitted the direct probe of single strand stationary equilibrium behavior. Simultaneously, the blooming of nanotechnology in the last 10 years made possible the detection of polymer properties in nonequilibrium conditions for which scaling theories provide almost no predictions.

Parallel to the improvements in nanofabrication, the understanding of confined polymers behavior has become an extremely attractive topic, and the reasons subtending such an increasing interest are many. First, conformations and dynamics of biopolymers are often affected by confinement in real living systems:[11,12] examples are provided by actin in cytoplasm,[13] DNA segregation in bacterial chromosomes,[14] and DNA packing in eukaryotic chromosomes,[15] bacterial spores,[16] and tail tubes.[17−19] Hence, understanding both polymers conformational statics and dynamics in simplified nanoenvironments, serves as a first step toward the comprehension of confinement effects in complex living systems. Second is the applicative approach. The fundamental advantage offered by nanodevices is in its capability to alter the equilibrium conformation from a coiled state to a stretched one, which is crucial in many applications, ranging from a fast genome length detection,[20] to biomolecular mixtures separation,[21−23] to single molecule mapping.[24,25] Third, the understanding of confinement effects on polymeric systems is fundamental also from a statistical mechanics point of view. Indeed experimental evidence may help to asses the validity of polymers models, underlying hypothesis and ensuing scaling relations. This happens in equilibrium conditions, where both static quantities such as end-to-end extension,[26−28] gyration radius[29−31] and the effect of the ionic strength on the equilibrium conformation[32,33] have shown a good agreement with the predicted scaling, and for dynamical equilibrium observables such as diffusion coefficient[31,34−36] and relaxation times[27,29,31,34−36] (and related ionic effects,[37]) which helped to confirm the results of de Gennes' scaling theory, a part from minor corrections due to the partial blobs draining.[36] However, recently these seemingly discrepancies have been reconciled with the usual blob theory by introducing correlations at the persistent length scale.[38] Polymer dynamics has been studied in nonequilibrium conditions as well:[39,40] extension and relaxation of molecules indeed have been shown to be drastically affected by electrophoretic[41−43] or hydrodynamic flows,[44−46] as well as the strand mobility.[23,47−49]

Surprisingly, compared to the progress on the experimental side, and despite its fundamental and practical importance, the theoretical understanding of the force-induced chain deformation in confinements remains behind. The swelling of the molecule arising from the action of an external force, indeed, is well-understood only in bulk conditions, where linear[8] and nonlinear[50] force−extension regimes were anticipated long before the celebrated Marko−Siggia formula.[51] In nanoenvironments, a quantitative study of the relationship between elongation and applied force heavily relies in numerical simulations.[52−56] In this paper, we furnish a detailed theoretical framework to establish the different regimes undergone by a polymer under tension trapped in a nanoslit. In doing so, our analysis sheds light on the existing intimate connection between channel and slitlike confinement conditions, providing the

Received: May 23, 2013
Revised: August 21, 2013
Published: September 16, 2013

natural linkage between the confinement-induced entropic forces that govern the strand's equilibrium and nonequilibrium dynamics.

The paper is outlined as follows. The first introductory part is devoted to recap the scaling properties of confined polymers in equilibrium conditions. The second section concerns the case of chains subject to the action of pulling forces in nanoslits: scaling theory and ensuing force−extensional regimes are discussed and derived within the correct thermodynamic formalism. Particular attention is devoted to the relation to tug-of-war experiments. Finally, in the ending section we compare and discuss the scaling preditions with respect to the experiments on polymer stretching and relaxation dynamics recently appeared in literature. In the Appendix, we report most of the analysis concerning channel equilibrium conditions.

EQUILIBRIUM IN CONFINEMENT CONDITIONS

In general, two limiting confinement conditions can be applied to a polymer: a quasi-biaxial or channellike confinement and a quasi-uniaxial or slitlike one.

Equilibrium in Channels. Since the main focus of the present work is on the scaling properties of slit-confined polymers, in this section we briefly overview the equilibrium conditions in channels, referring the reader to Appendix 6 for a more thorough analysis.

In quasi-biaxial confinement, the molecule configurational freedom is constrained in one dimensions, swelling inside a channel with circular, square or rectagular section. Different regimes can be defined according to the degree of confinement, which involves the competition between the length scales characterizing the polymer-channel physical system (see the recent review in[57] and references therein). Defining $R_{g,bulk}$ as the 3D bulk radius of gyration, P the polymer persistent length, and h the (average) channel size, two possible situations may arise: a moderate confinement, $R_{g,bulk} > h \gg P$, and a strong confinement $R_{g,bulk} > P \gg h$. In the first instance, referred to as the *de Gennes regime*, blob theory[2,10] requires that the polymer coils as it was free in bulk within a blob of size h: the chain is thus arranged as a sequence of repelling blobs whose number is

$$N_{blob} \simeq L\frac{(wP)^{1/3}}{h^{5/3}} \tag{1}$$

where L is the strand contour length and w its effective diameter. Moreover, the average end-to-end extension is given by

$$R^{deG}_{channel} \simeq L\frac{(wP)^{1/3}}{h^{2/3}} \tag{2}$$

When one of the two ends of a confined chain (even an infinitesimal portion) is free to coil in the bulk, it experiences the so-called recoiling force $f_{rec,channel}$, a force which is responsible for the translocation of the polymer out of the channel.[39,40] In the Appendix it is shown, by simple thermodynamic arguments, that

$$f^{deG}_{rec,channel} \simeq \frac{k_BT}{h} \tag{3}$$

which is independent from the end-to-end equilibrium length $R^{deG}_{channel}$ in agreement with refs.[39,40]

For small deviations from the channel equilibrium extension ($\delta R = R - R^{deG}_{channel}$), the molecule behaves as an entropic spring exerting an elastic restoring force toward the equilibrium condition $R^{deG}_{channel}$

$$f^{deG}_{el,channel}(R) \simeq -k^{deG}_{channel}(R - R^{deG}_{channel}) \tag{4}$$

with the spring stiffness given by[10,26,27]

$$k^{deG}_{channel} \simeq \frac{k_BT}{h^{1/3}L(wP)^{1/3}} \tag{5}$$

Notice that recoiling (eq 3) and elastic forces (eq 4) are mathematically well distinct as already stressed in ref 39.

The strong confinement condition is called the *Odijk regime*. In this case, the chain is composed by a sequence of *deflection rodlets* of linear size $\lambda \simeq h^{2/3}P^{1/3}$,[3] whose number is

$$N_\lambda \simeq \frac{L}{\lambda} = \frac{L}{P^{1/3}h^{2/3}} \tag{6}$$

and the chain displays an elongated equilibrium state which is N_λ times the average projection of a deflection segment along the channel axis:

$$R^{Odijk}_{channel} \simeq L\left[1 - A\left(\frac{h}{P}\right)^{2/3}\right] \tag{7}$$

A is a proportionality constant ≃0.17 or ≃0.18 in square and circular nanochannels, respectively.[58] Numerical simulations have confirmed the scaling in (eq 7).[58−62] In analogy to the de Gennes regime, it is possible to derive an expression for the recoiling force

$$f^{Odijk}_{rec,channel} \simeq \frac{k_BT}{P^{1/3}h^{2/3} - AP^{-1/3}h^{4/3}} \tag{8}$$

which is again independent of $R^{Odijk}_{channel}$ as in weak confinement conditions (see eq 3). For small displacements around the equilibrium extension (eq 7), on the score of an expansion similar to the de Gennes regime, the polymer experiences an elastic restoring force $f^{Odijk}_{el,channel}(R) \simeq - k^{Odijk}_{channel}(R - R^{Odijk}_{channel})$ with spring stiffness[27]

$$k^{Odijk}_{channel} \simeq \frac{k_BTP}{Lh^2} \tag{9}$$

Strong and moderate confinements, however, do not complete the set of possible regimes attained by a polymer trapped in a channel. Odijk[4] has argued that another regime arises in the transition region between Odijk and de Gennes confinement conditions: this situation, referred to as *extended de Gennes regime*,[57,61] applies when the degree of confinement is such that $2P < h < (P^2/w)$. As a matter of fact the extended de Gennes regime is characterized by a sequence of anisometric repelling blobs of size $H = ((hP)^{2/3}/w^{1/3})$ along the channel axis, a situation that considerably differs from the pure de Gennes case in which blobs of size h are totally isometric. The contour length stored in each anisometric blob turns out to be $(P^{1/3}h^{4/3}/w^{2/3})$, so that the number of blobs in which the molecule splits is

$$N_{ext-blob} \simeq L\frac{w^{2/3}}{P^{1/3}h^{4/3}} \tag{10}$$

The corresponding end-to-end equilibrium extension of the de Gennes regime (eq 2)

dx.doi.org/10.1021/ma4010549 | Macromolecules 2013, 46, 7989−8002

$$R_{channel}^{ext-deG} \simeq L\frac{(wP)^{1/3}}{h^{2/3}} \tag{11}$$

In analogy with weak and strong confinements, it is possible to write down the recoiling force in the extended de Gennes regime

$$f_{rec,channel}^{ext-deG} \simeq k_BT\frac{w^{1/3}}{(hP)^{2/3}} \tag{12}$$

We highlight that $f_{rec,channel}^{ext-deG}$ does not exhibit any dependence on $R_{channel}^{ext-deG}$ in full agreement with the expressions (eq 3) and (eq 8). In analogy to the de Gennes and Odijk regime the elastic force for small extensions $f_{el,channel}^{ext-deG}(R) \simeq -k_{channel}^{ext-deG}(R - R_{channel}^{ext-deG})$ with the corresponding spring constant[61]

$$k_{channel}^{ext-deG} \simeq \frac{k_BT}{PL} \tag{13}$$

Equilibrium in Slits. Uniaxial confinement corresponds to the polymer trapping in a quasi-2D environment: h in this case has the meaning of the slit height. In this situation the molecule curls up into a pancake whose shape in the unconfined directions is well described by an ellipse with radii R_m and R_M.[29−31,33,35] The direct imaging of the molecule equilibrium conformation yields the radius of gyration tensor, whose eigenvalues λ_m and λ_M are connected to the minor and major axis of the polymer ellipse by $R_m = (\lambda_m)^{1/2}$ and $R_M = (\lambda_M)^{1/2}$. Then, the strand in-plane radius of gyration can be defined as $R_{||} = 1/2(R_m^2 + R_M^2.)^{1/2}$ The theoretical approach to the equilibrium properties of a slit-confined molecule encompasses two limiting regimes as in the biaxial case: de Gennes ($h \gg P$) and Odijk ($h \ll P$).

In weak-to-moderate confinements, blob theory requires the polymer to behave as a 2D self-avoiding walk made of blobs of linear size h. The equilibrium end-to-end extension is given by[2]

$$R_{slit}^{deG} \sim hN_{blob}^{3/4} \sim L^{3/4}\left(\frac{Pw}{h}\right)^{1/4} \tag{14}$$

a result which is also obtained from a scaling ansatz.[2] Assuming the in-plane radius of gyration $R_{||} \sim R_{slit}^{deG}$, the predicted scaling has been confirmed by experiments[30,31,33,35] and numerical simulations.[63] The uniaxial confinement induces a free energy increase which coincides with that in nanochannels, eq 66[2]

$$\Delta F_{slit}^{deG}(R_{slit}^{deG}) = F_{slit}^{deG}(R_{slit}^{deG}) - F_{bulk}(R_{g,bulk}) \simeq k_BTN_{blob} = k_BT\left(\frac{R_{slit}^{deG}}{h}\right)^{4/3} \tag{15}$$

In analogy with biaxially confined molecules, it is possible to define the recoiling force $f_{rec,slit}^{deG}$ as the force that pulls the polymer into the bulk, when a small portion sticks out of the slit.[54] Since the dependence of the free energy on the blobs number N_{blob} is the same for channel and slitlike-confined polymers,[2] the chemical potential is identical in both conditions and it is furnished by eq 67. Accordingly, the recoiling forces coincide in chanels and slits; i.e., henceforth $f_{rec,slit}^{deG} = f_{rec,channel}^{deG} = f_{rec}^{deG} \simeq k_BT/h$ from eq 8.

For small deviations from the equilibrium end-to-end extension (eq 14), a second order expansion of the free energy attains the following form:

$$F_{slit}^{deG}(R) \simeq F_{slit}^{deG}(R_{slit}^{deG}) + \frac{1}{2}\left.\frac{\partial^2 F_{slit}^{deG}}{\partial R^2}\right|_{R=R_{slit}^{deG}}(R - R_{slit}^{deG})^2 \tag{16}$$

Hence, the free energy increment $\Delta F_{slit}^{deG}(R) = F_{slit}^{deG}(R) - F_{slit}^{deG}(R_{slit}^{deG})$ yields the following elastic restoring force

$$f_{el,slit}^{deG}(R) \simeq -k_{slit}^{deG}(R - R_{slit}^{deG}) \tag{17}$$

with a spring stiffness which has been shown by de Gennes[8] to be

$$k_{slit}^{deG} = -\left.\frac{\partial^2 F_{slit}^{deG}}{\partial R^2}\right|_{R=R_{slit}^{deG}} \simeq \frac{k_BT}{(R_{slit}^{deG})^2} = \frac{k_BTh^{1/2}}{L^{3/2}(Pw)^{1/2}} \tag{18}$$

In the Odijk regime, an argument similar to that of Flory for bulk polymers leads to a free energy of a R-extended chain equal to[4]

$$\frac{F(R)}{k_BT} \simeq \frac{R^2}{LP} + \frac{N_\lambda^2 v_\lambda}{R^2h} \tag{19}$$

where the number of deflection length is given in eq 6, and the excluded volume effects is defined in eq 70. Moreover, $\langle|\sin\delta|\rangle \simeq 1$ for infinite nanoslits.[4] Once minimized with respect to R, the expression (eq 19) yields the same end-to-end average elongation as the de Gennes expression (eq 14)

$$R_{slit}^{Odijk} \simeq L^{3/4}\left(\frac{Pw}{h}\right)^{1/4} \tag{20}$$

The former result has been corroborated by the experimental evidence,[35] once one assumes the in-plane gyration radius to exhibit the same scaling as the equilibrium end-to-end distance; i.e., $R_{||} \sim R_{slit}^{Odijk}$. Hence, attempting a 2D self-avoiding walk description, one obtains

$$R_{slit}^{Odijk} \simeq a_\lambda^{1/2}N_\lambda^{3/4} \tag{21}$$

where a_λ stands for the effective average area occupied by a deflection rod on the slit plane, i.e. $a_\lambda \sim P(hw)^{1/2}$. Again, one can write the free energy difference relative to the bulk equilibrium as

$$\Delta F_{slit}^{Odijk}(R_{slit}^{Odijk}) = F_{slit}^{Odijk}(R_{channel}^{deG}) - F_{bulk}(R_{g,bulk}) \simeq k_BT\left(\frac{Lw}{Ph}\right)^{1/2} \tag{22}$$

Note that, however, this scaling clearly differs from the expected confinement-induced increase of free energy, which must be identical to that valid in a channel up to numerical prefactors, i.e.

$$\Delta F_{slit}^{Odijk}(R_{slit}^{Odijk}) \simeq k_BTN_\lambda \simeq k_BT\frac{(R_{slit}^{Odijk})^{4/3}}{P^{2/3}(hw)^{1/3}} \tag{23}$$

see eq 71. Correspondingly we have that the recoiling force f_{rec}^{Odijk} is the same as in nanochannels, whose expression is furnished in eq 8.

A second warning on the use of eq 22 comes from the second order expansion around the equilibrium (eq 20), which yields an elastic force $f_{el,slit}^{Odijk}(R) \simeq -k_{slit}^{Odijk}(R - R_{slit}^{Odijk})$ with stiffness

$$k_{slit}^{Odijk} = -\left.\frac{\partial^2 F_{slit}^{Odijk}}{\partial R^2}\right|_{R=R_{slit}^{Odijk}} \simeq \frac{k_B T}{LP} \tag{24}$$

consistent with a mean field approximation. However, the well-known de Gennes' critique to mean field theory,[8] valid in 2D as well,[2] requires that

$$k_{slit}^{Odijk} \simeq \frac{k_B T}{(R_{slit}^{Odijk})^2} = \frac{k_B T h^{1/2}}{L^{3/2}(Pw)^{1/2}} \tag{25}$$

The evidence of the extended de Gennes regime is only numerical and pertains to the biaxial confinement.[61] However, experiments carried out under slitlike conditions well within the range of validity of this regime[35] ($2P < h < (P^2/w)$) have assessed no deviation from the theoretical scalings predicted by blob and Odijk theory respectively, i.e.

$$R_{slit}^{ext-deG} \simeq L^{3/4}\left(\frac{Pw}{h}\right)^{1/4} \tag{26}$$

in agreement with eqs 14 and 20. As a matter of fact, any attempt to draw a mean field Flory-like free energy in 2D is questionable,[1,8] and scaling arguments or self-avoiding random walk frameworks may better serve to explain the behavior in 26. Indeed, one can define $R_{slit}^{ext-deG} \simeq a_{ext-blob} N_{ext-deG}^{3/4}$ where $a_{ext-blob} \simeq (P^{1/2}h^{3/4}/w^{1/4})$ corresponds to the average area occupied by an anisotropic blob on the slit plane. On the other hand, a simple thermodynamic analysis suggests that the free energy increase due to the uniaxial confinement must exhibit the same scaling form as that obtained in channels, namely $\Delta F_{slit}^{ext-deG}(R_{slit}^{ext-deG}) = F_{slit}^{ext-deG}(R_{slit}^{ext-deG}) - F_{bulk}(R_{bulk}) \simeq k_B T N_{ext-blob}$. As a consequence, the recoiling force $f_{rec}^{ext-deG}$ coincides with the channel expression in eq 12.

Finally for small deviations from the equilibrium end-to-end extension (eq 26) the elastic force is $f_{el,slit}^{ext-deG}(R) \simeq -k_{slit}^{ext-deg}(R - R_{slit}^{ext-deG})$ with stiffness

$$k_{slit}^{ext-deG} \simeq \frac{k_B T}{R_{slit}^{ext-deG}} = \frac{k_B T h^{1/2}}{L^{3/2}(Pw)^{1/2}} \tag{27}$$

which recovers expressions (eq 18) and (eq 25).

FORCE STRETCHING IN NANOSLITS

Henceforth our analysis will focus on the action of an external force pulling a slitlike confined polymeric strand. However, before to proceed further to display our scaling framework, we need to specify the assumptions that our analysis will stem from, and the numerical and experimental evidence which it will be recovering.

Let us consider a polymer confined in a nanoslit and an external force $f_{el,slit}$ pulling both free ends: our goal is to obtain an expression for the polymer stationary extension R attained under the action of such a stretching. Theoretically, the desired force−extension relation could be obtained within the framework of the worm like chain model (WLC), where the relevant Gibbs free energy can be written as[54]

$$G_{slit}(P, L, h, f_{el,slit}) = \frac{k_B T}{2}\int_0^L \mathrm{d}s\, P\left(\frac{\partial^2 \mathbf{r}(s)}{\partial s^2}\right)^2 + V(z(s), h) - f_{el,slit} R \tag{28}$$

Here s represents the curvilinear abscissa of the polymer backbone, $\mathbf{r}(s) \equiv \{x(s), y(s), z(s)\}$ are the Cartesian coordinates of the polymer infinitesimal segment ds, $R = \hat{x}[\mathbf{r}(L) - \mathbf{r}(0)]$ is the end-to-end extension along the $\hat{x}$ direction, and $V(z(s),h)$ incorporates the sterical interaction between the molecule and the slit walls. The thermodynamic properties of the polymer chain can be drawn from eq 28, which indeed represents the thermodynamic potential relevant to the statistical ensemble that we implicitely chose: *the constant-force ensemble*. As a matter of fact, if we fix the value of the external force $f_{el,slit}$, the corresponding increment in the free energy (eq 28) is given by $\Delta G_{slit}(P, L, h, f_{el,slit}) = G_{slit}(P, L, h, f_{el,slit}) - G_{slit}(P, L, h, 0)$, and the average end-to-end distance corresponds to

$$\langle R \rangle = -\frac{\partial G_{slit}}{\partial f_{el,slit}} \tag{29}$$

In the following, we will neglect the fluctuations around the mean value and we will assume $R \simeq \langle R \rangle$. Experiments on stretching polymers are usually performed by fixing one end of the polymer and attaching the other to a bead which is then pulled by various means (magnetic, optical, mechanical, etc.). In such experiments one either fix the force on the bead and then measure the average polymer extension, or can constrain the bead position and look for the average force on the polymer: in the former instance one chooses the constant-force ensemble and the corresponding Gibbs free energy (eq 28), and in the second one chooses the constant-extension ensemble and the Helmholtz free energy $F_{slit}(P, L, h, R)$ as the relevant thermodynamic potential. The Flory free energies (eq 65), (eq 73) and (eq 19) are examples of Helmholtz thermodynamic potentials in nanochannels. If one wants to derive the elastic force needed to stretch a molecule by an extension R, one has to define the corresponding increment of the Helmholtz free energy $\Delta F_{slit}(P, L, h, R) = F_{slit}(P, L, h, R) - F_{slit}(P, L, h, R_{\|})$ and derive the elastic force through

$$f_{el,slit} = \frac{\partial F_{slit}}{\partial R} \tag{30}$$

on the score of what has been done in the previous section to obtain the spring stifnesses when small elongations are applied (see eqs 18, 25 and 27). Generally speaking, the constant-force ensemble is easier to treat theoretically and indeed data on force−extension experiments for bulk polymers[64] have been explained using this ensemble.[51] Anyhow, in the thermodynamic limit, both representations are equivalent, and the corresponding potentials are connected by the usual Legendre transform $G_{slit} = F_{slit} - f_{el,slit}R$. Comparing the former Legendre transform to eq 28 yields the exact analytical expression for the Helmholtz free energy furnished by the WLC:

$$F_{slit}(P, L, h, R) = \frac{k_B T}{2}\int_0^L \mathrm{d}s\, P\left(\frac{\partial^2 \mathbf{r}(s)}{\partial s^2}\right)^2 + V(z(s), h) \tag{31}$$

where the explicit dependence on R is expressed via $R = \hat{x} \cdot [\mathbf{r}(L) - \mathbf{r}(0)]$. For a complete discussion on the connection between the two statistical descriptions for finite chains in bulk see refs 65−67. Unfortunately, in spite of the rigorous analytical definition, expression (eq 28) is of a very limited usefulness to extract even an approximated force-extesion relation: it is not clear indeed how to treat the interaction term $V(z(s), h)$. Note

that the adoption of eq 31 simplifies this task. To complicate the situation, there are no, to the knowledge of the authors, sophisticated experimental apparatuses able to provide force−extension data in either one of the statistical ensembles.

Numerical simulations, however, may supply the necessary help in this sense. As a matter of fact, the only attempt to derive a force−extension relation for any degree of stretching R, is based on Brownian dynamics simulations. A modified worm like chain (mWLC) expression of the form

$$f_{el,slit}(R) \simeq \frac{k_B T}{l_c(h)}\left\{\frac{1}{4}\left[\frac{L^2}{(L-R)^2} - \frac{L^2}{(L-R_{||})^2}\right] + \frac{(R-R_{||})}{L}\right\} \tag{32}$$

has been suggested in ref 54. The in-plane radius of gration $R_{||}$ may correspond to eq 14, eq 20, or eq 26, depending on the confinement regime that the molecule undergoes, and the quantity $l_c(h)$ is defined as the polymer segmental correlation length in the unconfined directions.[55] Albeit in principle eq 32 provides the required force−extension relation, it is of less practical use, owing to the fact that the dependence of l_c on h is nontrivial and requires a numerical evaluation.

Because of the lack of a dedicated experimental tool, stretching experiments in nanoslits are performed using external hydrodynamic or electric field to pull the molecule out. In ref 43, an electric field was used to stretch a DNA molecule in slit confinement under de Gennes regime. The authors could demonstrate the existence of two distinct regimes during the relaxational dynamics once the field was off. These regimes were well characterized by different time scales and were attributed to distinct phases in the conformational changes toward the equilibrium (eq 14). The smaller time scale is that who drives the molecule rearrengement to an anisotropic configuration, where blobs are still aligned to the direction of the stretching electric field initially applied. The second corresponds to the rearrangement of blobs as a 2D self-avoiding chain. The existence of two distinct time scales ruling the dynamics of confined DNA has been confirmed subsequentely in cross-slot devices[42] and in hydrodynamic flows[44] where a two-stage coil−stretch transition was clearly observed.

Moreover, in a recent experiment,[54] we designed a micro/nanofluidic device which allowed us to probe the force−extension curve (eq 32) and the ensuing scaling, for a specific couple $(R, f_{el,slit})$ in the strong stretching limit. In this experiment, a DNA molecule straddles a nanoslit of length l_s, while both extremities are free to coil into two symmetric microchannels (see Figure 1). The conformational entropy difference at the micro-to-nano interfaces induces two opposite and equal recoiling forces f_{rec}, which pull the DNA portion in the nanoslit as a rope during the *tug-of-war*. Eventually one of the two ends wins, and the looser translocates to the winner side. We are interested to the portion of DNA trapped into the slit during the tug-of-war, i.e. the "rope". It is clear that its contour length fluctuates while its extension R is kept fixed, being equal to the slit length l_s in the x direction (see Figure 1). The proper statistical ensemble for the rope conformation is similar to a grand canonical ensemble for gases, with an average number of blobs, deflection legths or extended blobs set by the values of the chemical potential μ defined in eqs 67, 72, or 75,

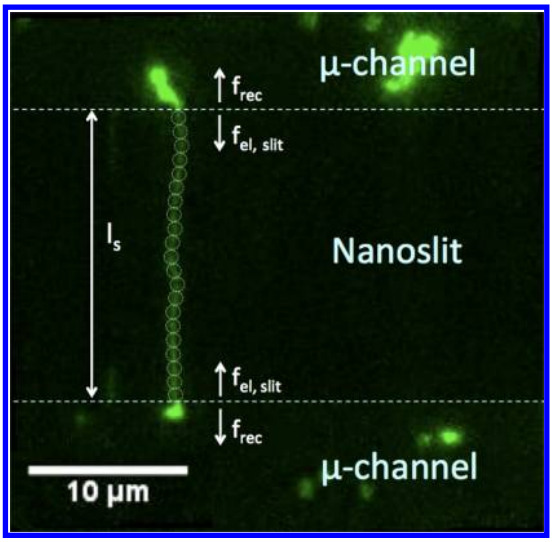

Figure 1. Typical configuration of DNA during the tug-of-war experiment.[54] Both molecular free ends coil inside the microchannels, exerting two opposite and equal entropic forces f_{rec} to the portion of DNA trapped inside the nanoslit (the "rope" of the tug-of-war). Correspondingly the external forces are counterbalanced by the elastic forces at the interfaces $f_{el,slit}$. The confined DNA has an average contour length L, and its extension R coincides with the length of the slit l_s. They are connected by the linear relation $l_s \equiv R = \alpha_{channel}(h)L$, see Table 1. The typical configuration of the DNA confined portion resembles the quasi-one dimension equilibrium condition of a polymer in a nanochannel ($l_s \equiv R \simeq R_{channel}$): dashed circles represent the pancakes in which the molecule can be subdivided at the onset of the channellike behavior.

respectively. The thermodynamical potential for this ensemble is $H_{slit}(P, h, R, f_{rec})$ and, in the thermodynamic limit ($L/P \gg 1$) and equilibrium conditions, its statistical description is equivalent to that furnished by eqs 28 and 31. In particular, the following Legendre transforms hold

$$H_{slit}(P, h, R, f_{rec}) = F_{slit}(P, h, R, L) - f_{rec}R_{channel} \tag{33}$$

$$H_{slit}(P, h, R, f_{rec}) = G_{slit}(P, h, R, f_{el,slit}) + f_{el,slit}R - f_{rec}R_{channel} \tag{34}$$

The latter equality has been achieved thanks to

$$\begin{aligned} \mu_{blob}N_{blob} &= f_{rec}^{deG}R_{channel}^{deG} && \text{de Gennes} \\ \mu_{\lambda}N_{\lambda} &= f_{rec}^{Odijk}R_{channel}^{Odijk} && \text{Odijk} \\ \mu_{ext-blob}N_{ext-blob} &= f_{rec}^{ext-deG}R_{channel}^{extdeG} && \text{extended de Gennes} \end{aligned} \tag{35}$$

which immediately follow from eqs 1−2, 6−7, and 10-11 respectively. Now, from eq 34, the requirement that H_{slit} must be independent of $f_{el,slit}$ gives

$$f_{el,slit} = -f_{rec} \tag{36}$$

and

$$R \simeq R_{channel} \tag{37}$$

In view of eq 36, in ref 54 we aimed at determining the scaling of f_{rec} for different slit confinements h, plugging in the formula (eq 32), the experimental measurables of the DNA trapped in the slit, i.e., L, and the corresponding values of $l_c(h)$ extracted

dx.doi.org/10.1021/ma4010549 | Macromolecules 2013, 46, 7989−8002

from numerical simulations in the range 40 nm <h < 110 nm (see Table 1). The experimental evidence suggested that the

Table 1. Values of the Parameters Relevant to the Tug-of-War Experiment[a]

h	l_c (nm)	$R_\parallel/L$	$\alpha_{channel}$	B_0 ($10^{-21}J$)	B_1 (nm^{-1})	B_2
40	123	0.74	0.88	6.32	15.48	0.69
50	112	0.67	0.85	3.73	5.19	0.60
65	100	0.64	0.84	4.06	4.67	0.58
110	81	0.54	0.75	3.28	1.14	0.43

[a]The values of the segmental correlation legth $l_c(h)$ are obtained from numerical simulations, while values of $R_\parallel/L$ and $\alpha_{channel}(h)$ are extracted from experimental data.[54] B_0, B_1, and B_2 are fitting parameters of the mWLC formula (eq 32) in the linear and nonlinear regions, respectively (see Figure 3).

average countour length of the confined DNA portion L and its elongation R (the slit length l_s), are bridged together by the linear relation

$$R = \alpha_{channel}(h)L \tag{38}$$

where the detected relative extensions, or degrees of stretching $\alpha_{channel}(h) = R/L$, are reported in Table 1. Comparing eq 37 and (eq 38) we have $R_{channel} \simeq \alpha_{channel}(h)L$, which is confirmed by eqs 2, 7, and 11. Once evaluated through eq 32, the elastic (and recoiling) force exhibited the following scaling

$$f_{el,slit}(R = \alpha_{channel}(h)L) \sim h^{-1} \tag{39}$$

The aim of this paper is to furnish a comprehensive scaling framework suitable to capture the different regimes of the force−extension relationship observed in the experiments, and able to recover the observed scaling (eq 39) when $R \simeq R_{channel}$.

Scaling Analysis of Stretched Polymers in Nanoslits. In this section we describe the regimes attained by the confined polymeric strand while subject to an external force $f_{el,slit}$. Tracing Pincus,[50] let us introduce a "tensile screening longitudinal length"

$$\xi_\parallel = \frac{k_B T}{f_{el,slit}} \tag{40}$$

Indeed, when applying $f_{el,slit}$, we can subdivide the polymeric chain into pancakes of pricipal axes ξ_M and ξ_m in the unconfined directions, and h along $\hat{z}$ (Figure 2b). In analogy to the in-plane radius of gyration, the tensile screening length is defined as $\xi_\parallel = 1/2\sqrt{\xi_M^2 + \xi_m^2}$ (Figure 2b1).

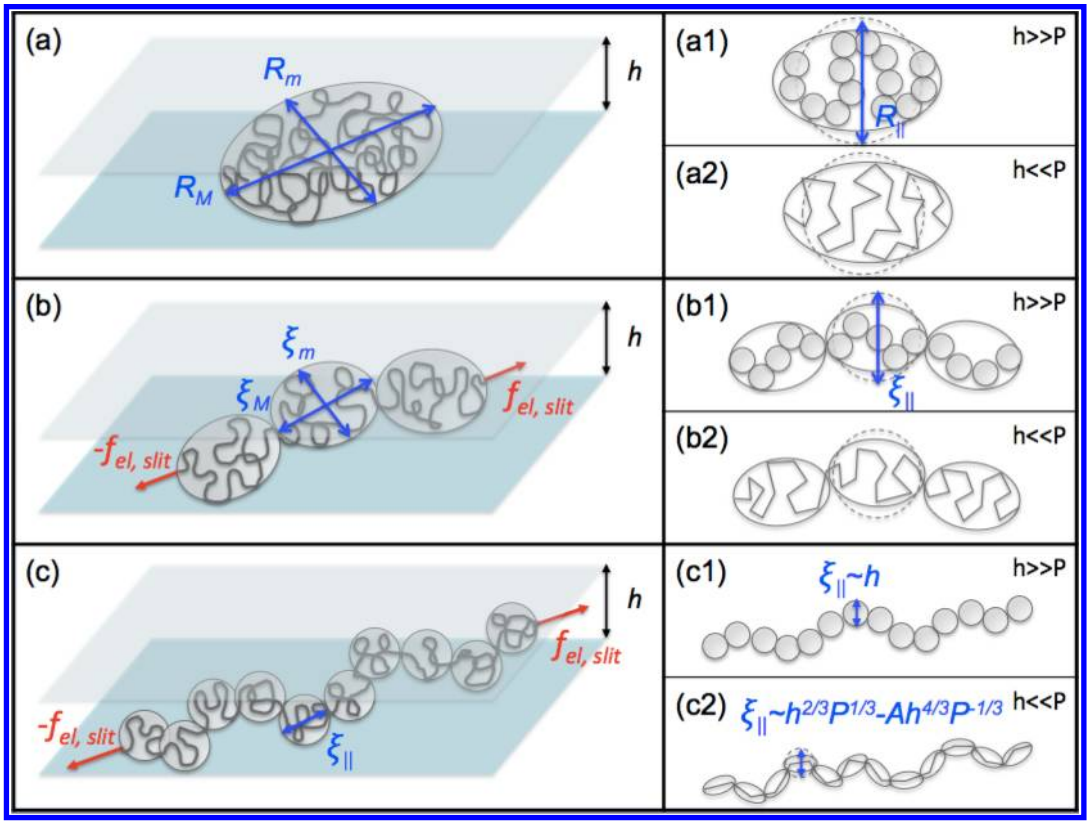

Figure 2. Schematic representation of the stretched DNA in a slit of height h. Panel a: the equilibrium configuration is a pancake with axis R_M, R_m and height h. The corresponding in-plane radius of gyration $R_\parallel$ is portrayed as a dashed circle in the de Gennes (a1) and Odijk regimes (a2). Panel b: DNA undergoing a severe stretching. The molecule consists of a sequence of pancakes of axis ξ_M, ξ_m and height h, inside which the polymer is considered in equilibrium. The average size of a pancake $\xi_\parallel$ is the dashed circle in the de Gennes (b1) and Odijk regime (b2). Panel c: crossover to a channellike behavior. The DNA stable configuration is a quasi-linear sequence of spherical blobs of size h in case of de Gennes molecules (c1); i.e., the transition entails a morphological change from anisotropic pancakes to isometric blobs. Panel c2: channellike configuration in the Odijk regime consists of an assembly of aligned rodlets: each rodlet has a projection, $\lambda[1 - A(h/P)^{2/3}]$, that nearly equals the tensile screening length $\xi_\parallel$ (dashed circles in panel c2). Morphological transition in this case does not occur and the pancake anisotropy is replaced by rodlet anisotropy. This anisotropy persists in the extended de Gennes regime, where the equilibrium configuration in the corresponding $h \times h$ channel is given in eq 11. In this case transition occurs when $\xi_\parallel \simeq H = ((hp)^{2/3}/w^{1/3})$.

dx.doi.org/10.1021/ma4010549 | Macromolecules 2013, 46, 7989−8002

For small extensions R, i.e., $R \sim R_{\parallel}$, the excluded volume interactions cannot be neglected in weak as well as in strong confinements. Therefore, we can expect that an hookean relation such that

$$f_{el,slit} \simeq k_B T \frac{(R - R_{\parallel})}{|R_{\parallel}^2|} \tag{41}$$

holds in the range of small external forces $f_{el,slit}$ i.e. for $\xi_{\parallel} \gg R_{\parallel}$ The linear force−extension relation (eq 41) entails that the spring constant is $k_{slit} \simeq (k_B T/R_{\parallel}^2)$ in analogy to eqs 18, 25, and 27 once we assume that $R_{\parallel} \simeq R_{slit}^{deG}$, $R_{\parallel} \simeq R_{slit}^{Odijk}$, and $R_{\parallel} \simeq R_{slit}^{ext\text{-}deG}$, respectively.

A second regime originates if we increase the force such that $R \gg R_{\parallel}$: the polymer starts unwinding and the tensile length shortens, i.e., $\xi_{\parallel} \ll R_{\parallel}$ but $\xi_{\parallel} \gg h$. Thus, we can subdivide the stretched molecule in several pancakes, inside which the DNA can be considered in equilibrium (Figure 2b).

Figure 2b1 represents the de Gennes case: the number of blobs within each pancake is $n_{blob}(\xi_{\parallel}) \sim (\xi_{\parallel}/h)^{4/3}$ from eq 14. It follows that the number of pancakes in which the molecule splits is $N_{\parallel} = (N_{blob}/n_{blob}(\xi_{\parallel})) \sim (R_{slitde}^{deG}/\xi_{\parallel})^{4/3}$.

The Odijk regime offers roughly the same picture (Figure 2b2). The number of deflection rods composing a pancakes is $n_{\lambda}(\xi_{\parallel}) \sim (\xi_{\parallel}/\sqrt{a_{\lambda}})^{4/3}$ from eq 21, and the total number of pancakes turns out to be $N_{\parallel} = (N_{\lambda}/n_{\lambda}(\xi_{\parallel})) \sim (R_{slitde}^{Odijk}/\xi_{\parallel})^{4/3}$.

Same argument can be applied to the extended de Gennes regime. As a matter of fact, since the average effective area occupied by an anisometric blob on the slit plane is $a_{ext-blob} \sim Ph^{3/2}w^{-1/2}$, the number of blobs inside a tension pancake reads $n_{ext-blob}(\xi_{\parallel}) \sim (\xi_{\parallel}/\sqrt{a_{ext-blob}})^{4/3}$. Thus, the total number of pancakes composing the extended chain is given by $N_{\parallel} = (N_{ext-blob}/n_{ext-blob}(\xi_{\parallel})) \sim (R_{slitde}^{ect-deG}/\xi_{\parallel})^{4/3}$.

The physics is thus the same in de Gennes, Odijk, and extended de Gennes regimes. Indeed, the swelling of the molecule weakens the excluded volume effects between blobs or deflection lengths belonging to different pancakes. In other words, excluded volume interactions between pancakes become less and less important as f_{el} grows. Hence, the DNA planar projection can be viewed as an ideal 2D chain composed by pancakes, for which we expect

$$R \sim N_{\parallel}\xi_{\parallel} \tag{42}$$

where

$$N_{\parallel} \sim \left(\frac{R_{\parallel}}{\xi_{\parallel}}\right)^{4/3} \tag{43}$$

Raising further $f_{el,slit}$, the effects due to the excluded volume between blobs or deflection lengths keep decreasing. In de Gennes regime, the tensile screening length shortens until it reaches the value of the slit height: $\xi_{\parallel} \sim h$. Correspondingly the pancakes become less eccentric, i.e. $\xi_M/\xi_m \to 1$ as $\xi_M, \xi_m \to h$: the pancakes are converging to spherical blobs. This morphological transition happens when the number of pancakes roughly correspond to the number of self-avoiding blobs, i.e., $N_{blob} \simeq N_{\parallel}$ (Figure 2c1). In this condition, the polymer is composed by blobs mostly aligned as if they were in a nanochannel, namely the conformation attained by the polymer at this crossover is nearly that attained at the equilibrium in a h-sized square channel

$$R \sim R_{channel}^{deG} \tag{44}$$

See eq 2. A further increase of the external force will have the only effect to contract isotropically the spherical blobs, until the steric effects of the slit walls become negligible. This scenario corresponds to that suggested by the relaxation experiment in ref 43. Indeed, the faster dynamical phase observed during the contracting process lasts from a degree of stretching $R/L \simeq 0.3$ to $R/L \simeq 0.08$, and is dictated by a time constant τ_I. The corresponding relaxation mechanism occurs while tension-blobs are almost perfectly aligned in the direction of original stretch. In this stage interactions with the confining walls can be considered negligible. The crossover to the slower process, with time constant τ_{II}, occurs when blobs span the height of the channel ($R/L \simeq 0.8$) to, i.e., $\xi_{\parallel} \simeq h$ (see Figure 2c1).

In the Odijk regime, the decay of the excluded volume effects entails the progressive alignment of the rods along $f_{el,slit}$ (Figure 2c2). Correspondingly, the random walk picture which led to eq 21, and which we kept valid within any tension-pancake, works less and less as $f_{el,slit}$ grows. The notion of a_{λ} becomes meaningless as $\langle |\sin \delta| \rangle \neq 1$, i.e. the strand attains an anisotropic configuration which is getting toward the nano-channellike equilibrium condition, for which $\langle |\sin \delta| \rangle \simeq (P/h)^{2/3}$. The latter is achieved whenever $\xi_{\parallel}$ nearly equals the average projection of a rod in the direction of $f_{el,slit}$: $\xi_{\parallel} \simeq \lambda[1 - A(h/P)^{2/3}] = h^{2/3}P^{1/3} - Ah^{4/3}P^{-1/3}$. Correspondingly, $N_{\lambda} \simeq N_{\parallel}$ and the end-to-end elongation approximately overlaps the equilibrium configuration in a nanochannel

$$R \simeq R_{channel}^{odijk} \tag{45}$$

where $R_{channel}^{Odijk}$ is furnished in eq 7. Once the crossover with the channellike configuration has been reached, however, increasing $f_{el,slit}$ to a greater extent does involve the fading of the steric interactions with the slit walls.

If the molecule is undergoing the extended de Gennes regime, the transition occurs when the extended blob size is roughly that of a tension-pancake with $\xi_{\parallel} \simeq H = ((Ph)^{2/3}/w^{1/3})$. Hence, we expect $N_{\parallel} \simeq N_{ext-blob}$, where the number of exteded blobs is given in eq 10, and

$$R \simeq R_{channel}^{ext-deG} \tag{46}$$

with $R_{channel}^{ext-deG}$ given in eq 11. As in de Gennes and Odijk regimes, raising further the elastic force has the only effect to regain the force−extension relation which is valid in bulk conditions.

To sum up, from eqs 44, 45, and 46 we can write down the scaling relation at the onset of channellike beavior:

$$R \sim R_{channel} \sim L \tag{47}$$

The different regimes arising from the outlined scenario can be wrapped up into a compact scaling form such as

$$R \sim R_{\parallel}\phi\left(\frac{R_{\parallel}}{\xi_{\parallel}}\right) \tag{48}$$

According to the previous analysis, the function $\phi(x)$ must be defined such that the following requirements are fulfilled:

1. $R \sim R_{\parallel}^2\xi_{\parallel}^{-1}$ if $\xi_{\parallel} \gg R_{\parallel}$, in order to recover eq 41.
2. $R \sim R_{\parallel}^{4/3}\xi_{\parallel}^{-1/3}$ from eq 42, if $h \ll \xi_{\parallel} \ll R_{\parallel}$ in de Gennes regime; $h^{2/3}P^{1/3} - Ah^{4/3}P^{-1/3} \ll \xi_{\parallel} \ll R_{\parallel}$ in the Odijk regime; $(Ph)^{2/3}w^{-1/3} \ll \xi_{\parallel} \ll R_{\parallel}$ in the extended de Gennes regime.

dx.doi.org/10.1021/ma4010549 | Macromolecules 2013, 46, 7989−8002

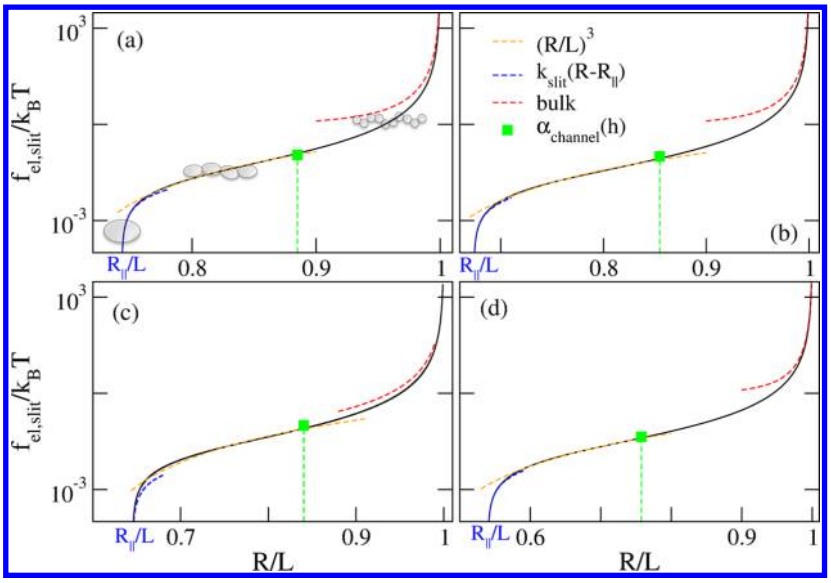

Figure 3. mWLC force−extension curves (in black) as resulting from eq 32 for h = 40 nm (a), h = 50 nm (b), h = 65 nm (c) and h = 110 nm (d); P = 66 nm. Corresponding values for $l_c(h)$ and $R_\parallel/L$ are furnished in Table 1. Dashed blue lines represent eq 41 through the fit $B_0(R - R_\parallel)/R_\parallel^2$. Orange lines stand for the nonlinear scaling (eq 49): the fitting function used is $B_1(R/L - B_2)^3$. See Table 1 for the numerical values of the fitting parameters. Green symbols pinpoints the values of $R/L = \alpha_{channel}(h)$ at which the elastic force has been calculated in the tug-of-war experiment (see Table 1). Red dashed lines correspond to the bulk WLC expression in ref 51.

3 $R \sim L$ from eq 47, if $\xi_\parallel \simeq h$ in de Gennes regime; $\xi_\parallel \simeq h^{2/3}P^{1/3} - Ah^{4/3}P^{-1/3}$ in the Odjik regime; $\xi_\parallel \simeq (Ph)^{2/3}w^{-1/3}$ in the extended de Gennes regime.

From the first requirement, it turns out that $\phi(x)$ for $x \ll 1$. When $x \gg 1$, a scaling form of the type $\phi(x) \simeq x^\beta$, yields $\beta = (1/3)$: this value indeed satisfies both second and third conditionsl i.e., it captures the very streteched regime $R \gg 1$ up to the onset of the channellike behavior.

Force−Extension Relationship. In this section, we specify the arguments emerged from the previous scaling analysis, to evaluate a force−extension relation in different regimes. In particular, our benchmark is the mWLC formula (eq 32).

In the linear regime, eq 41 captures the force extension behavior for $R \simeq R_\parallel$ as shown in Figure 3 (dashed blue lines).

In the moderate-to-high stretching regime, the invertion of eq 42 yields

$$f_{el,slit} \simeq \frac{k_BTh}{Pw}\left(\frac{R}{L}\right)^3 \tag{49}$$

thanks to eq 43, to eq 14, eq 20, or eq 26, and to the definition in eq 40. Hence, the elastic restoring force exhibites a strong nonlinear dependence on the extension R. We notice that the expression (eq 49) drastically differs from the bulk nonlinear force−extension regime where the Pincus' tension-blob scaling analysis gives $f_{el,bulk} \sim R^{3/2}$.[50] Most importantly, the scaling behavior (eq 49) reproduces the mWLC curve (eq 32) in the region $R \gg R_\parallel$ where the pancakes picture is supposed to apply (orange dashed lines in Figure 3), namely until the onset of the one-dimensional regime (green squares in Figure 3).

Let us turn to the transition to the channellike regime provided by eq 47. We have highlighted how this crossover corresponds to the quasi-1D polymer conformation, which separates the two exponential decays in the relaxation experiment reported in ref 43. On the other hand, eq 37 corresponds to eq 47, meaning that the DNA undergoes exactly this stretching regime while straddling the nanoslit in tug-of-war experiments.

First we address the de Gennes case. The onset of the one-dimensional blob sequence has been interpreted as a morphological transition of the tension-pancakes to isometric blobs. This happens when $\xi_\parallel \simeq h$, i.e.

$$f_{el,slit}^{deG} \simeq \frac{k_BT}{h} \tag{50}$$

from the definition (eq 40). The former expression confirms and explains the observed scaling of the elastic force as arising from tug-of-war eq 39 (see Figure 1 and Figure 4a). As a matter of fact, as required by eq 36, eq 50 matches the recoiling force expression (eq 3). The corresponding elongation R is

$$R \simeq L\frac{(Pw)^{1/3}}{h^{2/3}} \tag{51}$$

obtained by substituting the scaling expression $\phi\ (R_{slit}^{deG}/\xi_\parallel) = (R_{slit}^{deG}/\xi_\parallel)^{1/3}$ in (eq 48) and making use of eq 14 and of the equality $\xi_\parallel \simeq h$.

In the Odijk case, the requirement $\xi_\parallel \simeq h^{2/3}P^{1/3} - Ah^{4/3}P^{-1/3}$ yields

$$f_{el,slit}^{Odijk} \simeq \frac{k_BT}{h^{2/3}P^{1/3} - Ah^{4/3}P^{-1/3}} \tag{52}$$

from eq 40. Although the h^{-1}-dependence seems to provide a very good fit of the tug-of-war data, expression 52 describes fairly well the experimental observations in Figure 4a, in the range $h \leq 65$ nm. Yet, eq 52 is identical to eq 8 as required by relation 36. Furthermore, in this case, the length attained by the polymer when the quasi-1D transition takes place is

$$R \simeq L\left[1 - A\left(\frac{h}{P}\right)^{2/3}\right] \tag{53}$$

when substituting eq 7 in eq 45. We note that a scaling form such as (eq 48) is no longer rigorous in the Odijk regime. Indeed, substituting $\phi\ (R_{slit}^{deG}/\xi_\parallel) = (R_{slit}^{deG}/\xi_\parallel)^{1/3}$ in (eq 48), and making use of eq 20 together with $\xi_\parallel \simeq h^{2/3}P^{1/3} - Ah^{4/3}P^{-1/3}$,

dx.doi.org/10.1021/ma4010549 | Macromolecules 2013, 46, 7989−8002

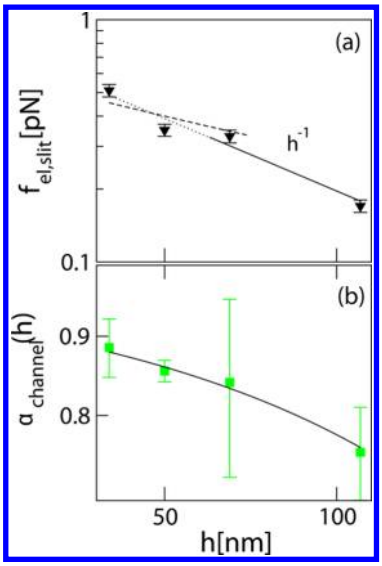

Figure 4. Scaling theory and comparison with experimental results. Panel a: experimental values of the elastic force $f_{el,slit}$ and the corresponding fits with the expressions 50 and 52 in the de Gennes and Odijk regimes, respectively. For h in the de Gennes domain, we fitted with (B_3/h) with $B_3 = 19.61 \pm 0.06 \times 10^{-21} J$ (solid and dotted black line), while for $h \leq 65$ nm we have used $(B_4/(h^{2/3}P^{1/3} - Ah^{4/3}P^{-1/3})$ with $P = 66$ nm and $A = 0.169$ as in panel (b), getting $B_4 = 18.86 \pm 0.01 \times 10^{-21}$ J (dashed black line). Note that assuming a room temperature of 300K, $k_BT \simeq 4.14 \times 10^{-21} J$ which is in reasonable agreement with B_3 and B_4. Panel (b): green squares are the experimental values of $\alpha_{channel}(h)$ for different slit confinement h as arising from tug-of-war experiments[54] (see Table 1). eq 53 requires that $\alpha_{channel}(h) \simeq [1 - A(h/P)^{2/3}]$ at the crossover to a channellike behavior in the Odijk regime: fitting data with this law ($P = 66$ nm) gives $A = 0.169 \pm 0.007$ (solid black line) in excellent agreement with numerical simulations.[58]

does not recover eq 53. This can be explained by the fact that scaling arguments only work when the number of deflection lengths inside a pancake, is large enough that the ansatz of self-similarity between tension-pancake and overall equilibrium conformation applies.

Finally, if the confinement is such that the molecule is in the extended de Gennes regime, the relation $\xi_\parallel \simeq H = ((Ph)^{2/3}/w^{1/3})$ automatically yields

$$f_{el,slit}^{ext-deG} \simeq \frac{k_B T_w^{1/3}}{(Ph)^{2/3}} \tag{54}$$

while the end-to-end average elongation is

$$R \simeq L\frac{(wP)^{1/3}}{h^{2/3}} \tag{55}$$

from eqs 46 and 14. Although the average elongations 51 and 55 are equivalents in de Gennes and extended de Gennes regimes, the elastic forces exhibit different scalings at the onset of channellike behavior, as it results by a direct comparison of eqs 50 with 54. Furthermore, eq 54 is equivalent to the recoiling force 12 as required by the equality 36. As in the Odijk confinement, plugging eq 14 in ϕ $(R_{slit}^{ext-deG}/\xi_\parallel) = (R_{slit}^{ext-deG}/\xi_\parallel)^{1/3}$ gives an average end-to-end extension which differs from eq 55, pointing out that the scaling form (eq 48) is no longer adequate to describe the channellike polymer conformation under stronger stretching in the extended de Gennes regime.

From eqs 51, 53, and 55 it is possible to extract the degree of stretching of a molecule during the tug-of-war, i.e., when the channel transition sets on: $\alpha_{channel}(h) = R/L \simeq R_{channel}/L$. In Figure 4b, we fitted the experimental values of $\alpha_{channel}(h)$ arising from tug-of-war experiments, using the expression $\alpha_{channel}(h) \simeq [1 - A(h/P)^{2/3}]$ valid in the Odijk regime (eq 53). The best fit gives $A \simeq 0.17$ in excellent agreement with the numerical simulations in nanochannels.[58] However, since both de Gennes and extended de Gennes regimes furnish $\alpha_{channel}(h) \sim h^{-2/3}$ (see, eqs 51 and 55), a general expression encompassing strong and weak confinment limits could be eq 55

$$\alpha_{channel}(h) \simeq \frac{1}{1 + A\left(\frac{h}{P}\right)^{2/3}} \tag{56}$$

which is plotted in Figure 5.

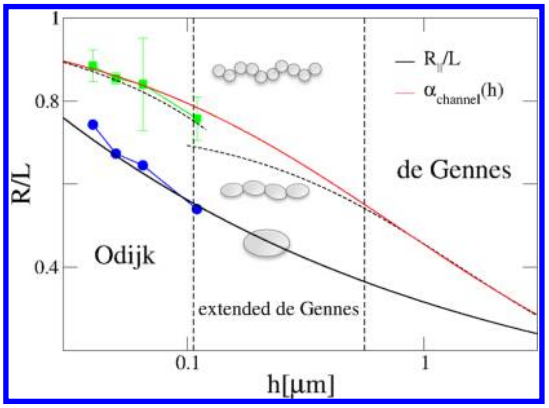

Figure 5. Polymer relative extension R/L as a function of the degree of confinement h. Red curve represents the transition to channellike configuration, i.e. $\alpha_{channel}(h) = (1/[1 - A(h/P)^{2/3}])$ which merges Odijk (eq 56), extended de Gennes (eq 55) and de Gennes formula (eq 51), respectively. $A = 0.169$ as arising from the fit of Figure 4a. However eqs 56 and 51 are plotted for the reader's convenience (black dashed lines). Green symbols stand for the relative extensions of the DNA portion inside the slit during tug-of-war experiments (see Table 1). Black solid curve represents the relative equilibrium $R_\parallel/L$ eq 57, and has been obtained as the best fit of the tug-of-war data reported in 1 (blue symbols), by means of the function $(1/C_0h^{1/4})$ with $C_0 = 0.25 \pm 0.04$. Linear behavior of force−extension is expected to apply close to red and black functions, i.e., eqs 58 and 41, respectively. The nonlinear bulk regime holds above the red line, while the nonlinearity $f_{el} \sim R^3$ in eq 49 is valid within the region between the red and black curves.

As said, the nonlinear force−extension approximation (eq 49) ceases to work as the nanochannel configuration sets on. Indeed, in Figure 3 orange lines deviates from the mWLC curves (eq 32) for $R/L > \alpha_{channel}(h)$ (green symbols).

After the transition to the channellike regime has occurred, the effects of the confining slit walls become less and less important as $f_{el,slit}$ increases. In the (extended) de Gennes picture, the (extended) tension-blobs shrink progressively. The Odijk picture, instead, describes the polymer as a sequence of aligned rodlets whose deflection angles rapidly approach 0. Henceforth, the bulk behavior is recovered and the usual WLC force−extension relation applies[51] (red dashed lines in Figure 3).

dx.doi.org/10.1021/ma4010549 | Macromolecules 2013, 46, 7989−8002

DISCUSSION AND RELATION TO COIL−STRETCH TRANSITION

Let us discuss the physical picture emerging from our scaling analysis with the support of the plot in Figure 5, where the average relative extension R/L is shown as a function of the confinement h. Plot is ideally divided in three vertical regions, each pertaining to its corresponding confining conditions. It is also divided in two horizontal regions by two equilibrium curves: $\alpha_{channel}(h) \simeq R_{channel}/L$, given by eq 56, accounting for the average fractional length of a polymer in a channel, and the slit equilibrium ratio $R_{||}/L$ that reads

$$\frac{R_{||}}{L} \simeq \left(\frac{Pw}{Lh}\right)^{1/4} \tag{57}$$

from eqs 14, 20, and 26. Blue symbols represent the values of the relative equilibrium DNA extension from tug-of-war experiments, as reported in Table 1. Black curve has been drawn for the reader's convenience only, since it is apparent from eq 57 its explicit dependence on $L^{-1/4}$. For values of the relative extension R/L above the curve $\alpha_{channel}(h)$, the polymer is in the bulk stretching regime and no sterical interactions with the confinement walls hinder its motion. Inside the region between the curves 56 and 57, the effects of the slit confinement on the polymer conformational dynamics are strong. The region below the black curve is unaccessible, since $R_{||}$ represents the average gyration radius of the polymer under uniaxial confinement.

Once the value of the nanoslit height has been chosen, relaxation experiment such that reported in ref.,[43] is done by tracing a vertical line from the top of the plot to the black curve: indeed the drawn line represents $R(t)/L$, the retracting average end-to-end extension (normalized to the polymer contour length L) toward the slit equilibrium condition. By crossing the red curve from above, the polymer enters a first linear regime of the force−extension relationship. As a matter of fact, our scaling arguments have shown that at the crossover to the channellike behavior, the elastic force coincides with the recoiling force and, remarkably, this force is independent of the polymer elongation R as it turns out from formulas 50, 52, and 54. Therefore, it is eligible to perform a first order expansion of the elastic force around $R \simeq R_{channel}$

$$f_{el,slit}(R) \simeq f_{rec} - \left.\frac{\partial f_{el,slit}}{\partial R}\right|_{R=R_{channel}} (R - R_{channel}) \tag{58}$$

Now let us put in the following ansatz: in the vicinity of the channel equilibrium extension, the slit retracting force can be decomposed in $f_{el,slit}(R) \simeq {}_{frec} + f_{el,channel}(R)$. Hence, we can expect that

$$\left.\frac{\partial f_{el,slit}}{\partial R}\right|_{R=R_{channel}} \simeq k_{channel} \tag{59}$$

We are assuming that the polymer behaves as a biaxially confined molecule while crossing the channel crossover, pictured by the red line in Figure 5. Now, in the relaxation experiment reported in ref 43, the decay of the function $(R(t)/L)^2 - (R_{||}/L)^2$ was detected and fitted with the exponential $\sim e^{-(t/\tau)}$. Such an exponential behavior is usually achieved by imposing a linear expression of the driving force. As stressed previously, two separate exponentials were found with two characteristic times, τ_I and τ_{II}, therefore indicating the presence of two linear regimes of the elastic force responsible for the polymer contraction. Thanks to eqs 58 and 59, we argue that the shorter characteristic time is given by $\tau_I = \zeta/k_{channel}$, where ζ is the polymer drag coefficient. Usually, the drag on a polymeric chain is solely dependent on the drag on a polymer segment times the number of segments composing the chain. Hence

$$\zeta_{blob} \sim hN_{blob} \simeq L\frac{(wP)^{1/3}}{h^{2/3}} \tag{60}$$

in the de Gennes confinement conditions,[2,10] where we made use of eq 1. Correspondingly the Odijk regime yields[27,68]

$$\zeta_{\lambda} \sim \frac{\lambda}{\log(h/w)}N_{\lambda} \simeq \frac{L}{\log(h/w)} \tag{61}$$

thanks to eq 6. In the extended de Gennes regime the drag coefficient is equivalent to the de Gennes case, i.e.

$$\zeta_{ext-blob} \sim HN_{ext-blob} \simeq L\frac{(wP)^{1/3}}{h^{2/3}} \tag{62}$$

Therefore, using eqs 5, 9, and 13 together with eqs 60, 61, and 62, respectively, we obtain

$$\tau_I \simeq \begin{cases} \dfrac{(hL)^2}{k_BT\,\log(h/w)P} & \text{Odijk} \\ \dfrac{L^2P^{4/3}w^{1/3}}{k_BTh^{2/3}} & \text{extended de Gennes} \\ \dfrac{L^2(Pw)^{2/3}}{k_BTh^{1/3}} & \text{de Gennes} \end{cases} \tag{63}$$

In the relaxation experiment reported in ref 43, the authors calculated a relative extension $\alpha_{channel}(h) \simeq 0.08$ for $h = 1\ \mu$m at this crossover channel-to-slit, while plot in Figure 5 suggests that for the same height the channel equilibrium relative extension should be approximately 0.5. However, as suggested by the authors, the crossover extension, as well as the equilibrium extension $R_{||}$, strongly depend on solvent quality, ionic strength and temperature. Moreover they observed a scaling $\tau_I \simeq h^{-1/2}$, which slightly differs from the proposed scaling in eq 63 under de Gennes regime $h^{-1/3}$. On the other hand, the detection of the channel characteristic time scale τ_I is controversial, experiments done under biaxial confinement conditions for 140 nm < h < 440 nm[27] yielded $\tau_I \simeq h^{-0.9\pm0.4}$, in agreement to the corresponding extended de Gennes regime formula;[61] numerical simulations, however, have shown deviations from the predicted scaling in de Gennes regime.[53,69−71]

In the region between red and black equilibrium curves in Figure 5, the driving elastic force is nonlinear as reported in eq 49. Hence no exponential decay is expected. However, linear regime is soon recovered close to the slit equilibrium, when the relative extension $(R(t)/L) \rightarrow (R_{||}/L)$, as provided by eq 41. The characteristic time scale τ_{II} ruling the last part of relaxation is equal to ζ/k_{slit}, where the spring stiffness is given by eqs 18, 25 and 27 in the de Gennes, Odijk, and extended de Gennes regime, respectively. Hence, using for the chain drag the expressions 60, 61, or 62, the lower relaxation time is

dx.doi.org/10.1021/ma4010549 | Macromolecules 2013, 46, 7989−8002

$$\tau_{II} \simeq \begin{cases} \dfrac{L^{5/2}(Pw)^{1/2}}{k_B T h^2 \log(h/w)} & \text{Odijk} \\ \dfrac{L^{5/2}(Pw)^{5/6}}{k_B T h^{7/6}} & \text{extended de Gennes} \\ \dfrac{L^{5/2}(Pw)^{5/6}}{k_B T h^{7/6}} & \text{de Gennes} \end{cases} \quad (64)$$

This time corresponds to the longest conformal relaxation time in most single-molecule studies, albeit its scaling under de Gennes confinement has been shown to be slightly weaker than that predicted by Brochard.[9,34,36] The two exponentials behaviors in the relaxational dynamics, with characteristic times (eq 63 and eq 64), can be clearly distinguished only when red and black curves are well separated in the plot of Figure 5. For example, there can be no clear separation between the exponential decays for $h \simeq 2$ μm, where both linear regimes occur around $R/L \simeq 0.3$; remarkably, this is the same relative extension for the onset of linear regime when a molecule retracts in bulk.[72]

Stretching experiments consist in drawing a vertical line upside-down, from the bottom black curve to the top of the plot in Figure 5. A stretch can be applied by means of an ideal external force $f_{el,slit}$ as described in the former section, or by electric field or hydrodynamic flow.[42,44] In the experiment reported in[42] a T4 DNA molecule was placed in an homogeneous extensional electric field under varying degree of confinement, 150 nm < h < 2 μm. In these conditions the relative extension $R(t)/L$ is a function of the applied electrophoretic strain $\epsilon\dot{t}$, where $\dot{\epsilon}$ is the fixed strain rate. After an initial time T, the relative extension reaches a stationary value which strongly depends on the strain rate through the Deborah number De, defined as $\epsilon\dot{t}$, where τ represents the polymer's typical relaxation time. In bulk conditions, the existence of a sharp coil−stretch transition has been observed around $De \simeq 0.5$;[73] i.e., a sudden increase of the stationary R/L value is detected when the strain rate applied is such that $\dot{\epsilon} \simeq 0.5/\tau$. Since under uniaxial confinement there are two characteristic times, two Deborah numbers can be defined $De_I = \epsilon\dot{t}_I$ and $De_{II} = \epsilon\dot{t}_{II}$ and two coil−stretch transitions can be expected at different strain rates $\dot{\epsilon} = cinst_1/\tau_I$ and $\dot{\epsilon} = cinst_2/\tau_{II}$. In the cited experiment,[42] only the coil−stretch transition pertaining to the first Deborah number $De_I \simeq 0.5$ could be reported. The same authors, however, in a subsequent experiment performed by using hydrodynamic flow to stretch the DNA strand,[44] demonstrated both coil−stretch transitions, although that corresponding to $De_{II} \simeq \text{const}_2$ could be clearly observed only for shallow nanoslits.

For bulk polymers, the abrupt coil−stretch transition is closely related to the onset of a linear trend in the force−extension relation. As a matter of fact, the hookean elastic force is balanced by the hydrodynamic drag force exerted on the molecule by the elongational flow, when the strain rate is $\dot{\epsilon} \simeq 0.5/\tau$. In potential flow theory, this is interpreted in terms of a conformational energy landscape that becomes flat near the coil−stretch transition;[74] i.e., a large number of configurations corresponding to vastly different end-to-end elongations are available for $De \simeq {}_{0.5}$. Theory and simulations have provided the evidence that the time T needed to reach the stationary relative extension R/L considerably increases while approaching the stretch-coil transition,[75,76] and, correspondingly, experiments have shown the existence of a peak in the standard deviation σ of the relative extension.[77] In nanoslits the presence of two linear regimes in the force−extension relationship, corresponding to the vicinity of black and red curves in Figure 5, entails the appereance of two peaks in the relaxation time T and in the standard deviation of the fractional extension distribution σ. In particular the location of both peaks of σ offers a quantitative criterion to determine the exact value of the Deborah numbers at which transitions occur.

The picture offered in Figure 5 may help in the understanding of the possible scenario arising in different regimes. For molecules under Odijk confinement regime, the slit equilibrium degree of stretching is very high, 0.75 < $R_{\parallel}/L$ < 0.5. At the same time, the channel linear regime characterizing the crossover to the channellike configuration happens around 0.8 < $\alpha_{channel}(h)$ < 0.9. Hence the linear approximation of the force−extension relation eq 58, is valid within a very limited range of R/L, since it is bounded from the above strong nonlinearity of the bulk regime, and from below by $f_{el} \sim R^3$ as in eq 49. This range consists of the extensional states for which the drag force counterbalances the elastic force (eq 58), and the narrower it is, the shallower is the corresponding peak in σ. On the other side, the linear regime (eq 41) in the vicinity of $R_{\parallel}/L$ involves a broad range of R/L, therefore it entails a pronounced second peak of σ. These features qualitatively correspond to the numerical results obtained in ref 44 using the dumbbell model. By increasing h, one goes from Odijk to the extended de Gennes regime and the channel spring stiffness $k_{channel}$ in eq 59 decreases, passing from eq 9 to eq 13. As a consequence, one would expect a significant increase of the first peak of σ. In this regime of confinement, both peaks in the standard deviation σ would be well-distinguished. Eventually, the peak corresponding to the channel linear regime (eq 58) becomes more pronounced than that pertaining to the equilibrium expansion (eq 41), yet closer. Well within the de Gennes regime it is almost impossible to separate both peaks, resulting in an unique extremely high value of standard deviation σ. The interval of R/L fulfilling a linear expansion of the force−extension relationship is very large indeed, merging to the bulk linear region as well ($R/L \simeq 0.3$), in agreement with the simulations reported in ref 44.

Future experiments could assess the validity and correcteness of our scaling theory and of the emerging physical picture. One possibility is represented by the experimental setup described in ref 56, where one of the two free ends of the DNA was immobilized and the other was attached to an external bead. However, particular attention must be paid to the fact that only a portion of the DNA is trapped in a nanoslit, and this fraction is not easily determined, leading to a rather difficult direct detection of $f_{el,slit}$ by means of the external tweezers. On the other hand, the transverse elastic modes analysis may shed light on the characteristic time scales scaling. Furthermore, new tug-of-war experiments, spanning a wider range of confinement h, could help to reconstruct the red curve in Figure 5, i.e., eq 56. Moreover, thanks to eqs 2, 7, and 11, the same (average) curve should be obtained by detecting the average relative elongation $R_{channel}/L$ of channel-confined polymers in equilibrium within the same degree of confinement. New relaxation and/or stretching experiments are needed to check whether the characteristic times governing the dynamics exhibit the predicted scaling in 63 and 64. In particular, it appears that only in the extended de Gennes regime the two linear-force phases are clearly separated by a nonlinear regime. In this case,

dx.doi.org/10.1021/ma4010549 | Macromolecules 2013, 46, 7989−8002

the curve $R(t)/L$ of a retracting molecule, for example, should show two exponentials decays bridged by a behavior similar to $R(t) \sim t^{-1/2}$. Finally, one could imagine to perform a relaxation experiment in channel, and compare the time constant emerging from an exponential fit close to the equilibrium condition, to the corresponding τ_I coming from relaxational dynamics experiments performed in nanoslits.

CONCLUSIONS

We have furnished a detailed analysis of the scaling regimes undergone by a slit-confined polymer under tension. Our framework provides the evidence of three distinct regimes of the force−extension curve: linear, nonlinear, and bulk-like, reproducing the mWLC formula in the corresponding regions. The transition to the bulk condition, when almost no sterical confinement hinders the polymer motion, is achieved when the polymer's conformation roughly corresponds to the one-dimensional assembly of (extended) blobs or deflection lengths. Remarkably, the elastic force at this crossover equals the recoiling force in the corresponding h-sized nanochannel equilibrium configuration; i.e., it does not exhibit any dependence on the elongation R. Moreover we have provided the evidence of two linear regimes in force−extension curve: one close to the slit equilibrium condition and the other at the onset of the channellike configuration. This two linear regimes account for several observed features in relaxation and stretching experiments, ranging from distinct exponential decays, to the appeareance of two stretch-coil transitions. We have also provided the scaling expressions for the characteristic times dictating the polymer's dynamics and for the spring stiffnesses characterizing both linear regimes. Our study allows to shed light on the close relationship between polymer dynamics under uniaxial and biaxial confining conditions and, most importantly, it provides the suitable scaling framework able to reproduce the outcomes of recent experiments performed in very different conditions.

APPENDIX

In this appendix, we furnish detailed explanations of most of the formula appearing in the introductory section regarding equilibrium in nanochannels.

In the de Gennes regime, recently a Flory-type free energy has been introduced to recover the static properties of polymers undergoing channellike confinement[52,53]

$$\frac{F^{deG}_{channel}(R)}{k_BT} \simeq \frac{R^2}{h^2 N_{blob}} + \frac{hN^2_{blob}}{R} \tag{65}$$

Minimization with respect to R yields the end-to-end extension given in eq 2, which exactly corresponds to the expression furnished by de Gennes, $R^{deG}_{channel} \simeq hN_{blob}$,[2,10] and which has been confirmed by Monte Carlo[78−80] and Langevin simulations.[69,81] By substituting eq 2 into eq 65, one can see how the confinement induces a free energy increase relative to the bulk equilibrium

$$\Delta F^{deG}_{channel}(R^{deG}_{channel}) = F^{deG}_{channel}(R^{deG}_{channel}) - F_{bulk}(R_{g,bulk}) \simeq k_BT\frac{R^{deG}_{channel}}{h} \tag{66}$$

that matches the result obtained by the blob theory for which $\Delta F^{deG}_{channel}(R^{deG}_{channel}) \simeq k_BTN_{blob}$, as follows from eq 1.[2,10]Such an increase in the free energy has a clear entropic origin: indeed, it is attributed to the drastic reduction of the polymer allowable configurations due to the channel confinement. The confinement-induced depletion of the phase space justifies also the appeareance of the so-called recoiling force $f_{rec,channeb}$ a force which is responsible for the translocation of the polymer out of the channel, if one of the two ends (even an infinitesimal portion) is free to coil in the bulk[39,40] The above argument provides an intuitive picture of the entropic nature of the recoiling process, but does not furnish, however, a scaling expression for $f^{deG}_{rec,channel}$ An analytical form of the recoiling force can be derived from the expression (eq 65), thanks to simple thermodynamic arguments in step with blob theory. Indeed, the natural thermodynamic variables of the Flory's free energy $F^{deG}_{channel}$ are intensive (the temperature T), and extensive (R and L). Blob theory allows to replace the contour length with the number of blobs N_{blob} thanks to eq 1, so that we can express $F^{deG}_{channel}(T, R, N_{blob}) \simeq k_BTN_{blob}$. Hence, it is possible to write

$$\frac{\partial F^{deG}_{channel}}{\partial N_{blob}} = \mu_{blob} \simeq k_BT \tag{67}$$

where μ_{blob} is the chemical potential, or free energy per blob, which can be interpreted as $\mu_{blob} \simeq f^{deG}_{rec,channel}h$. From eq 67, the recoiling force attains the expression (eq 3).

For small deviations from the channel equilibrium extension ($\delta R = R - R^{deG}_{channel}$), the free energy (eq 65) can be approximated by a second order expansion

$$F^{deG}_{channel}(R) \simeq F^{deG}_{channel}(R^{deG}_{channel}) + = \frac{1}{2}\frac{\partial^2 F^{deG}_{channel}}{\partial R^2}\bigg|_{R=R^{deG}_{channel}} (R - R^{deG}_{channel})^2 \tag{68}$$

Hence the elastic restoring force is obtained as

$$\frac{\partial F^{deG}_{channel}}{\partial R} = f^{deG}_{el,chaneel}(R) \tag{69}$$

whose expression is furnished in (eq 4). The spring constant expression (eq 5) is obtained by $k^{deG}_{channel} = -(\partial^2 F^{deG}_{channel}/\partial R^2)|_{R=R^{deG}_{channel}}$.

In the strong-confinement (Odijk) regime, the alignment of deflection rodlets along the channel imposes a drastic reduction of the excluded volume which can be written as

$$v_\lambda = \lambda^2 w\langle|\sin\delta|\rangle \tag{70}$$

where δ is the angle between two subsequent rods and $\langle|\sin\delta|\rangle \simeq (P/h)^{2/3}$ in nanochannels.[4] The confinement-induced free energy change with respect the bulk equilibrium is written as

$$\Delta F^{Odijk}_{channel}(R^{odijk}_{chaneel}) = F^{Odijk}_{channel}(R^{odijk}_{chaneel}) - F_{bulk}(R_{g,bulk}) \simeq k_BTN_\lambda = k_BT\frac{R^{Odijk}_{chanel}}{P^{1/3}h^{2/3} - AP^{-1/3}h^{4/3}} \tag{71}$$

In analogy to the de Gennes regime, we can define a chemical potential as

$$\frac{\partial F^{Odijk}_{channel}}{\partial N_\lambda} = \mu_\lambda = \simeq k_BT \tag{72}$$

where the Gibbs' free energy per deflection length is $\mu_\lambda \simeq f^{Odijk}_{rec,channel}(P^{1/3}h^{2/3} - AP^{-1/3}h^{4/3})$, as the quantity $P^{1/3}h^{2/3} - AP^{-1/3}h^{4/3}$ corresponds to the projection of the deflection length on the channel axis, i.e. $\lambda[1 - A(h/P)^{2/3}]$ Inserting this

dx.doi.org/10.1021/ma4010549 | Macromolecules 2013, 46, 7989−8002

definition into eq 72 we get an expression for the recoiling force (eq 8). For small displacements from the equilibrium configuration, the molecule experiences a Hookean force $f_{rec,channel}^{Odijk} \simeq -k_{channel}^{Odijk}(R - R_{channel}^{Odijk})$, where $k_{channel}^{Odijk}$ is given in eq 9.

In the intermediate extended-de Gennes regime, the free energy of a confined chain can be casted in the following Flory-type form

$$\frac{F_{channel}^{ext-deG}(R)}{k_BT} \simeq \frac{R^2}{N_{ext-blob}H^2} + H\frac{N_{ext-blob}^2}{R} \tag{73}$$

which, once minimized with respect to R, furnishes the same end-to-end equilibrium extension of the de Gennes regime (eq 2), i.e. expression (eq 11). In this regime the free energy increase due to the confinement is given by

$$\Delta F_{channel}^{ext-deG}(R_{chennel}^{ext-deG}) = F_{channel}^{ext-deG}(R_{chennel}^{ext-deG}) - F_{bulk}(R_{g,bulk}) \simeq \frac{k_BT\omega^{1/3}}{(hP)^{2/3}}R_{channel}^{ext-deG} \tag{74}$$

that corresponds to the scaling consistent to the extended-blob picture, i.e., $\Delta F_{channel}^{ext-deG}(R_{channel}^{ext-deG}) \simeq k_BTN_{ext-blob}$ thanks to the definition (eq 10). Hence, in analogy with weak and strong confinements, it is possible to write

$$\frac{\partial F_{channel}^{ext-deG}}{\partial N_{ext-deG}} = \mu_{ext-deG} \simeq k_BT \tag{75}$$

where we have introduced the free energy per extended blob $\mu_{ext\text{-}deG} \simeq f_{rec,channel}^{ext-deG}H$. The expression for the recoiling force eq 12 can be straightforwardly derived from eq 75 according to the procedure outlined in the de gennes and Odijk case. Expanding to the second order the extended de Gennes free energy (eq 74) yields an elastic force $f_{el,channel}^{ext-deG}(R)$ with the spring constant iven by $k_{channel}^{ext-deG} = -(\partial^2 F_{channel}^{ext-deG}/\partial R^2)|_{R=R_{channel}^{ext-deG}}$, whose expression is reported in eq 13. In this respect, it is interesting to note that the polymer elastic behavior for smalle displacements is similar to that of an unconfined chain, as $k_{bulk} \sim k_BT/(PL)$, and independent of the degree of confinement h. This intriguing behavior may be due to the fact that the excluded voleume effects in this case are played by the channel walls, while the corresponding molecule in bulk would behave as an ideal chain, being too short to feel the effects of self-avoidance (see the discussion in ref 57).

The situation, however, is even more complicated. Between Odijk and extended de Gennes, a transition regime encompasses a range of h where physical observables exhibit scalings typical of ideal chains. This transition region, defined as a *Gaussian de Gennes* regime,[62] had been predicted by Casassa almost 50 years ago[82] and observed in numerical simulations:[59,61,83−85] the free energy in this regime scales as $F_{channel} \sim (P/h)^2$ and the equilibrium end-to-end extension $R_{channel} \sim LP/h$ In the following, for the sake of clarity in the exposition and to avoid unnecessary complications, our analysis will not contemplate this transition regime, although it must be bear in mind that our scaling framework can be straightforwardly extended to it.

AUTHOR INFORMATION

Corresponding Authors

*E-mail: (A.T.) alessandro.taloni@gmail.com.

*E-mail: (C.-F.) cfchou@phys.sinica.edu.tw.

Notes

The authors declare no competing financial interest.

ACKNOWLEDGMENTS

A.T. acknowledges the financial support of the European Complexity-net pilot project "LOCAT". C.-F.C is grateful to the supports from AS Nano Program, AS Foresight Project (AS-97-FP-M02), and the National Science Council (Taiwan) (99-2112-M-001-027-MY3, 102-2112-M-001-005-MY3) and AFRL Asian Office of Aerospace Research & Development (FA2386-13-1-4023).

REFERENCES

(1) de Gennes, P. G. *Scaling Concepts in Polymer Physics*, 1st ed.; University Press: Ithaca, 1979.
(2) Daoud, M.; Azde Gennes, P. G. *J. Phys. (Paris)* **1977**, *38*, 85−93.
(3) Odijk, T. *Macromolecules* **1983**, *16*, 1340−1344.
(4) Odijk, T. *Phys. Rev. E* **2008**, *77*, 060901−1−4(R).
(5) Odijk, T. *J. Chem. Phys.* **2006**, *125*, 204904−1−8.
(6) Gompper, G.; Burkhardt, T. W. *Phys. Rev. A* **1989**, *40*, 6124−6127.
(7) Burkhardt, T. W. *J. Phys. A: Math. Gen.* **1997**, *30*, L167−L172.
(8) de Gennes, P. G. *Macromolecules* **1976**, *9*, 587−93.
(9) Brochard, F. *J. Phys. (Paris)* **1977**, *38*, 1285−1291.
(10) Brochard, F.; de Gennes, P. G. *J. Chem. Phys.* **1977**, *67*, 52−56.
(11) Marenduzzo, D.; Micheletti, C.; Orlandini, E. *Phys. Rep.* **2011**, *504*, 1−73.
(12) Zhou, H.; Rivas, G.; Minton, A. *Ann. Rev. Biophys.* **2008**, *37*, 375−397.
(13) Köster, S.; Pfohl, T. *Cell Motil. Cytoskeleton* **2009**, *66*, 771−776.
(14) Jun, S.; Mulder, B. *Proc. Natl. Acad. Sci. U.S.A.* **2006**, *103*, 12388−12393.
(15) Wolffe, A. *Chromatin: Structure and Function*, 1st ed.; Academic Press: London, 1998.
(16) Errington, J. *Microbiol. Rev.* **1993**, *57*, 1−33.
(17) Speir, J. A.; Johnson, J. E. *Curr. Opin. Struct. Biol.* **2012**, *22*, 65−71.
(18) Inamdar, M.; Gelbart, W.; Phillips, R. *Biophys. J.* **2006**, *91*, 411−420.
(19) Löf, D.; Schillén, K.; Jönsson, B.; Evilevitch, A. *J. Mol. Biol.* **2007**, *368*, 55−65.
(20) Levy, L. S.; Craighead, H. G. *Chem. Soc. Rev.* **2010**, *39*, 985−999.
(21) Han, J.; Craighead, H. G. *Science* **2000**, *288*, 1026−1029.
(22) Doyle, P. S.; Bibette, J.; Bancaud, A.; Viovy, J. L. *Science* **2002**, *295*, 2237−2237.
(23) Strychalski, E. A.; Lau, H. W.; Archer, L. A. *J. Appl. Phys.* **2009**, *109*, 024915−1−5.
(24) Chan, E. Y.; Goncalves, N. M.; Haeusler, R. A.; Hatch, A. J.; Larson, J. W.; Maletta, A. M.; Yantz, G. R.; Carsteal, E. D.; Fuchs, M.; Wong, G. G.; Gullans, S. R.; Gilmanshin, R. *Genome Res.* **2004**, *14*, 1137−1146.
(25) Jo, K.; Dhingra, D. M.; Odijk, T.; de Pablo, J. J.; Graham, M. D.; Runheim, R.; Forrest, D.; Schwartz, D. C. *Proc. Natl. Acad. Sci. U.S.A.* **2007**, *104*, 2673−2678.
(26) Tegenfeld, J. O.; Prinz, C.; Cao, H.; Chou, S.; Reisner, W. W.; Rien, R.; Yan, Y. M.; Cox, E. C.; Sturm, J. C.; Silberzan, P.; Austin, R. H. *Proc. Natl. Acad. Sci. U.S.A.* **2004**, *101*, 10979−10983.
(27) Reisner, W.; Morton, K. J.; Riehn, R.; Wang, Y. M.; Yu, Z.; Rosen, M.; Sturm, J. C.; Chou, S. Y.; Frey, E.; Austin, R. H. *Phys. Rev. Lett.* **2005**, *94*, 196191−1−4.
(28) Su, T.; Das, S. K.; Xiao, M.; Prashant, P. K. *PLoS 1* **2011**, *6*, 16890−1−9.
(29) Bonthuis, D. J.; Meyer, C.; Stein, D.; Dekker, C. *Phys. Rev. Lett.* **2008**, *101*, 108303−1−4.
(30) Strychalski, E. A.; Geist, J.; Gaitan, M.; Locascio, L. E.; Stavis, S. M. *Macromolecules* **2012**, *45*, 1602−1611.

(31) Lin, P.-K.; Fu, C.-C.; Chen, Y.-L.; Chen, Y.-R.; Wei, P.-K.; Kuan, C. H.; Fann, W. S. *Phys. Rev. E* **2007**, *76*, 011806−1−7.
(32) Reisner, W.; Beech, J. P.; Larsen, N. B.; Flyvbjerg, H.; Kristensen, A.; Tegenfeld, J. O. *Phys. Rev. Lett.* **2007**, *99*, 058302−1−4.
(33) Lin, P.-K.; Hsieh, C. C.; Chen, Y. L.; Chou, C. F. *Macromolecules* **2012**, *45*, 2920−2927.
(34) Balducci, A.; Mao, P.; Han, J. Y.; Doyle, P. S. *Macromolecules* **2006**, *39*, 6273−6281.
(35) Tang, J.; Levy, S. L.; Trahan, D. W.; Jones, J. J.; Craighead, H. G.; Doyle, P. S. *Macromolecules* **2010**, *43*, 7368−7377.
(36) Hsieh, C.-C.; Balducci, A.; Doyle, P. S. *Macromolecules* **2007**, *40*, 5196−5206.
(37) Hsieh, C.-C.; Balducci, A.; Doyle, P. S. *Nano Lett.* **2008**, *8*, 1683−1688.
(38) Dai, L.; Tree, D. R.; van der Maarel, J. R. C.; Dorfman, K. D.; Doyle, P. S. *Phys. Rev. Lett.* **2013**, *110*, 168105−1−5.
(39) Turner, S. W. P.; P. M., C.; Craighead, H. G. *Phys. Rev. Lett.* **2002**, *88*, 128103−1−4.
(40) Mannion, J. T.; Reccius, C. H.; Cross, J. D.; Craighead, H. G. *Bioph. J.* **2006**, *90*, 4538−4545.
(41) Bakajin, O. B.; Duke, T. A. J.; Chou, C.-F.; Chan, S. S.; Austin, R. H.; Cox, E. C. *Phys. Rev. Lett.* **1998**, *80*, 2737−2740.
(42) Balducci, A.; Tang, J.; Doyle, P. S. *Macromolecules* **2008**, *41*, 9914−9918.
(43) Balducci, A.; Hsieh, C. C.; Doyle, P. S. *Phys. Rev. Lett.* **2007**, *99*, 238102−1−4.
(44) Tang, J.; Trahan, D. W.; Doyle, P. S. *Macromolecules* **2010**, *43*, 3081−3089.
(45) Stein, D.; van der Heyden, F. H. J.; Koopmans, W. J. A.; Dekker, C. *Proc. Natl. Acad. Sci. U.S.A.* **2006**, *103*, 15853−15858.
(46) Larson, J. W.; Yantz, G. R.; Zhong, Q.; Charnas, R.; D'antoni, C. M.; Gallo, M. V.; Gillis, K. A.; Neely, L. A.; Phillips, K. M.; Wong, G. G.; Gullans, S. R.; Gilmanshin, R. *Lab Chip* **2006**, *6*, 1187−1199.
(47) Cross, J. D.; Strychalski, E. A.; Craighead, H. G. *J. Appl. Phys.* **2007**, *102*, 024701−1−5.
(48) Campbell, L. C.; J., M.; Wilkinson,; Manz, A.; Camilleri, P.; Humphreys, C. J. *Lab Chip* **2004**, *4*, 225−229.
(49) Salieb-Beugelaar, G. B.; Teapal, J.; van Nieuwkasteele, J.; Wijnperlé, D.; Tegenfeld, J. O.; Lisdat, F.; van den Berg, A.; Eijkel, C. T. *Nano Lett.* **2008**, *8*, 1785−1790.
(50) Pincus, P. *Macromolecules* **1976**, *9*, 386−388.
(51) Marko, J. F.; Siggia, E. D. *Macromolecules* **1995**, *28*, 8759−8770.
(52) Jun, S.; Thirumalai, D.; Ha, B.-Y. *Phys. Rev. Lett.* **2008**, *101*, 138101−1−4.
(53) Jung, Y.; Jun, S.; Ha, B.-Y. *Phys. Rev. E* **2009**, *79*, 061912−1−8.
(54) Yeh, J. W.; Taloni, A.; Chen, Y. L.; Chou, C. F. *Nano Lett.* **2012**, *12*, 1597−1602.
(55) Chen, Y. L.; Lin, P. K.; Chou, C. F. *Macromolecules* **2010**, *43*, 10204−10207.
(56) Lin, J.; Persson, F.; Fritzsche, J.; Tegenfeldt, J.; Saleh, O. *Biophys. J.* **2012**, *102*, 96−100.
(57) Reisner, W.; Pedersen, R. J.; Austin, R. H. *Rep. Prog. Phys.* **2012**, *75*, 106601−1−32.
(58) Yang, Y.; Burkhardt, T. W.; Gompper, G. *Phys. Rev. E* **2007**, *76*, 011804−1−7.
(59) Cifra, P. *J. Chem. Phys.* **2009**, *131*, 224903−224907.
(60) Burkhardt, T. W.; Yang, Y.; Gompper, G. *Phys. Rev. E* **2010**, *82*, 041801−1−9.
(61) Wang, Y.; Tree, D. R.; Dorfman, K. D. *Macromolecules* **2011**, *44*, 6594−6604.
(62) Tree, D. R.; Wang, Y.; Dorfman, K. D. *Phys. Rev. Lett.* **2013**, *110*, 208103−1−4.
(63) Chen, Y. L.; Graham, M. D.; de Pablo, J. J.; Randall, G. C.; Gupta, M.; Doyle, P. S. *Phys. Rev. E* **2004**, *70*, 060901−1−4 (R).
(64) Bustamante, C.; Marko, J. F.; Siggia, E. D.; Smith, S. *Macromolecules* **1994**, *265*, 1599−1600.
(65) Kreuzer, H. J.; Payne, S. H. *Phys. Rev. E* **2002**, *63*, 021906−1−4.
(66) Dhar, A.; Chauduri, D. *Phys. Rev. Lett.* **2002**, *89*, 065502−1−4.
(67) Samuel, J.; Sinha, S. *Phys. Rev. E* **2002**, *66*, 050801−1−4(R).
(68) Morse, D. C. *Macromolecules* **1998**, *31*, 7044−7067.
(69) Jendrejack, R.; Schwartz, D.; Graham, M.; Pablo, J. J. D. *J. Chem. Phys.* **2003**, *119*, 1165−1173.
(70) Arnold, A.; Bzorgui, B.; Frenkel, D.; Ha, B. Y.; Jun, S. *J. Chem. Phys.* **1992**, *96*, 4046−4052.
(71) Graham, M. D. *Ann. Rev. Fluid Mech.* **2011**, *43*, 273−298.
(72) Perkins, T. T.; Quake, S. R.; Smith, D. E.; Chu, S. *Science* **1994**, *264*, 822−826.
(73) Perkins, T. T.; Smith, D. E.; Chu, S. *Science* **1997**, *276*, 2016−2021.
(74) de Gennes, P. G. *J. Chem. Phys.* **1974**, *60*, 5030−5042.
(75) Vincenzi, D.; Bodenschatz, E. *J. Phys. A: Math. Gen.* **2006**, *39*, 10691−10701.
(76) Celani, A.; Puliafito, A.; Vincenzi, D. *Phys. Rev. Lett.* **2006**, *97*, 118301−1−4.
(77) Geraschenko, S.; Steinberg, V. *Phys. Rev. E* **2008**, *78*, 040801−1−4(R).
(78) Kremer, K.; Binder, K. *J. Chem. Phys.* **1984**, *81*, 6381−6394.
(79) Milchev, A.; Paul, W.; Binder, K. *Macromol. Theory Simul.* **1994**, *3*, 305−323.
(80) Wall, F. T.; Seitz, W. A.; Chin, J. C.; de Gennes, P. G. *Proc. Natl. Acad. Sci. U.S.A.* **1978**, *75*, 2069−2070.
(81) Jendrejack, R.; Dimalanta, E.; Schwarz, D.; Graham, M.; Pablo, J. J. D. *Phys. Rev. Lett.* **2003**, *91*, 038102−1−4.
(82) Casassa, E. W. *J. Polym. Sci., Part B: Polym. Lett.* **2013**, *110*, 168105−1−5.
(83) Cifra, P.; Benková, Z.; Bleha, T. *J. Chem. Phys. B* **2009**, *113*, 1843−1851.
(84) Cifra, P. *J. Chem. Phys.* **2012**, *136*, 024902−1−8.
(85) Dai, L.; Ng, S. Y.; van der Maarel, P. S. D. J. R. C. *ACS Macro Lett.* **2012**, *1*, 1046−1050.

NOTE ADDED AFTER ASAP PUBLICATION

This article published ASAP on September 16, 2013. References 41, 73, and 75 have been revised. The correct version posted on September 18, 2013.